J. Korean Soc. Ind. Appl. Math. Vol.27, No.1, 75–86, 2023 https://doi.org/10.12941/jksiam.2023.27.075

DESCRIPTIONS OF ATTACK ANGLE AND IDEAL LIFT COEFFICIENT FOR VARIOUS AIRFOIL PROFILES IN WIND TURBINE BLADE

JAEGWI GO

DEPARTMENT OF ELECTRICAL ENGINEERING, DONG-A UNIVERSITY , BUSAN 49315, REPUBLIC OF KOREA
E-mail address: sunpgo@dau.ac.kr

ABSTRACT. The angle of attack is highly sensitive to pitch point in the airfoil shape and the decline of pitch point value induces smaller angle of attack, which implies that airfoil profile possessing closer pitch point to the airfoil tip reacts more sensitively to upcoming wind. The method of conformal transformation functions is employed for airfoil profiles and airfoil surfaces are expressed with a trigonometric series form. Attack angle and ideal lift coefficient distributions are investigated for various airfoil profiles in wind turbine blade regarding conformal transformation and pitch point. The conformed angle function representing the surface angle of airfoil shape generates various attack angle distributions depending on the choice of surface angle function. Moreover, ideal attack angle and ideal lift coefficient are susceptible to the choice of airfoil profiles and uniform loading area. High ideal attack angle signifies high pliability to upcoming wind, and high ideal lift coefficient involves high possibility to generate larger electric energy. According to results obtained pitch point, airfoil shape, uniform loading area, and the conformed airfoil surface angle function are crucial factors in the determination of angle of attack.

1. INTRODUCTION

According to growing greenhouse emissions and global warming the exploitation of renewable and pollution free energies is significantly required to alternative fossil fuel energy. Representative sources of renewable energy are solar and wind. Wind energy has stood in the spotlight progressively due to the increased demand of scientific and industrial advancements, and wind supports possibly more that 20% of global electricity in the year of 2030 [1]. By the advantage of superior efficiency, wider operational range, and reliability, horizontal axis wind turbine (HAWT) is an example structure as a mass power production during the last several decades.

Flow field behaviors around wind turbine are very complicate owing to turbulence generation, vortices, and stall flow. Numerous research studies have investigated the aerodynamics occurring around wind turbines to understand the detailed process of kinetic energy extraction from wind. Blade element momentum (BEM) theory, Vortex method (VM), and Computational fluid dynamic (CFD) are widely known approaches. BEM is the combination of momentum and blade element theories by dividing the wind turbine blade into independent elements. The method is not appropriate for heavy loaded states, that is, the axial induction factor is greater than 0.5 [2, 3]. By adding the assumption of inviscid flow field to VM, the wind turbine blade and wake are regarded as vortex particles. The influences of tip

Received January 16 2023; Revised March 3 2023; Accepted in revised form March 4 2023; Published online March 25 2023.
2020 *Mathematics Subject Classification*. 74F10.
Key words and phrases. airfoil, attack angle, conformal transformation, ideal lift, mean line.

vortices can be predicted using VM, while it is difficult to investigate the effects of flow separation with VM [4, 5]. CFD is a mathematical process for solving the numerical solutions of complex nonlinear partial differential equations involving fluid flow. CFD enables to describe the physical phenomena of laminar, transitional, and turbulent flows. Moreover, the behavior of streamlines, pressure, and velocity contours as actual flow around a wind turbine can be described with the help of CFD [6], and CFD has been used widely to predict HAWT performances.

The determination of airfoil shape for wind turbine blades is fundamental task for designing wind turbine rotors [7]. Airfoil design in the wind turbine is to accomplish a high aerodynamic performance that produces high electric energy in the designed wind turbine. By virtue of computer technologies many numerical tools are developed to investigate the optimization states of airfoil shapes. Hicks et al. [8], Eppler[9], Tangler and Somers[10], are early authors to compose numerical optimization in airfoil design. Conformal mapping method and velocity distribution are taken into account to design airfoil shape by researchers [11, 12]. Echjijem and Djebli [13] considered the correction of the axial and tangential induction factors in the design of wind turbine blade, and Lim and Kim [14] studied multi-objective airfoil shape optimization using adaptive hybrid evolutionary algorithm. Lim and Kim found that the cases of lift maximum and high angle of attack show multi-modality in the design spaces. Tirandaz and Rezaeiha [15] investigated the optimal airfoil shape for vertical axis wind turbines in dynamic stall under the suffering of low tip speed ratio based on 252 high-fidelity transient CFD simulations of 126 identical airfoil shapes. By the application of free-form deformation technique to adjust the airfoil curve using control points, Hu et al. [16] reduced the dimension of control variables and found the sensitivity of lift-drag ratio and static stability height to vertical adjustments near the leading edge.

However, the separated design process of airfoil and blade fails to grant an optimum state, and integrated design of airfoil and blade is required. 2D airfoil and 3D integrated design approach is addressed by Sartori et al. [17]. The airfoil shape is designed to increase computational efficiency, whereas limited accessible airfoil geometry is appeared. Wang et al. [18] suggested an integrated method that describes airfoil profiles with a trigonometric series form and series of polynomial equations using conformal transformation. The method yields direct and accurate shapes of airfoil and airfoil shape is controlled by the coefficients in series. Wei et al. [19] presented an integrated method for designing airfoil families of large wind turbine blades. They included rotor diameter, tip speed ratio, and local speed ratio to express optimal airfoils, and a shape perturbation function is applied to the geometry of the prescribed airfoils. Kumar et al. [20] simulated airfoil shape for optimum wind characteristics using a computer program JAVAFOIL to drive the relationship of angle of attack with coefficients of lift and drag. Huang et al. [21] constructed bionic airfoil combined with the lever movement shape of the dolphin skeleton for the investigation of aerodynamic performance of horizontal axis wind turbine, presenting an improved results in the lift coefficients and noise characteristics. N$\acute{u}\tilde{n}$ez [22] applied an asymptotic expansion in powers of the airfoil width to study the shape of the cavity created in a conducting fluid by a magnetic field within a thin airfoil. But, most of previous works have analyzed numerically the influences of critical factors in the aerodynamic performance of specified airfoil shapes.

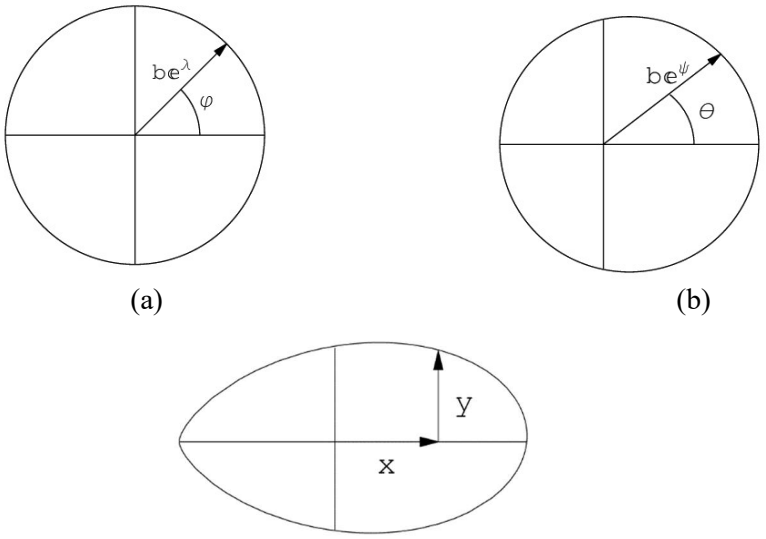

FIGURE 1. Schematic illustration of transformations to derive airfoils: (a) z-Plane, (b) z'-Plane, (c) ξ-Plane.

In the present study, by the method of conformal transformation functions for airfoil profiles and airfoil surfaces are expressed with a trigonometric series form, which depicts various airfoil profiles with the appropriate control of the coefficients of series. The attack angle distributions are described analytically around the circumference of various airfoil shapes and compared. Even, pitch point is controlled to clarify the differences of attack angle distributions. Ideal angle of attack and ideal lift coefficients are expressed by dint of the area of uniform for various airfoil profiles.

2. MATHEMATICAL MODELLING

2.1. **Airfoil profiles**. Any airfoil profiles can be obtained by a conformal transformation of a circle and expressed with Fourier expansions [19]. Let us define the coordinates of z and z' by, respectively,

$$z = be^{\lambda+i\varphi}$$
$$z' = be^{\psi+i\theta},$$

The coefficient b represents the radius of circular cylinder, be^{λ} the radius vector of z, φ the angular coordinate of z, be^{ψ} the radius vector of z', and θ the angular coordinate of z' (see Fig. 1). Due to the general transformation of z' relating to z plane given by

$$z' = z\,exp\left[\sum_{n=1}^{\infty}(A_n + iB_n)\frac{1}{z^n}\right],$$

the ψ and θ can be represented with

$$\psi(\varphi) = \lambda + \sum_{m=1}^{n-1}(A_m\,cos\,m\varphi + B_m\,sin\,m\varphi) + A_n\,cos\,n\varphi$$
$$\theta(\varphi) = \varphi - \sum_{m=1}^{n-1}(A_m\,sin\,m\varphi - B_m\,cos\,m\varphi) + A_n\,sin\,n\varphi.$$

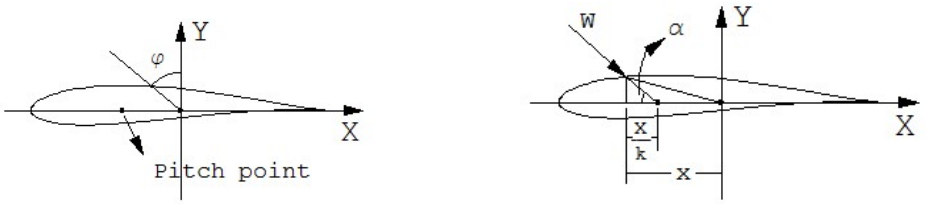

(a) (b)

FIGURE 2. Airfoil profile transformed of a circle by conformal mapping: (a) angle of surface, (b) relative flow angle onto blade.

With the values at the specified $2n$ equally spaced intervals in the range $0 \le \varphi \le 2\pi$, that is, $0, \frac{\pi}{n}, \frac{2\pi}{n}, \cdots, \frac{(2n-1)\pi}{n}$, the λ, A_m, and B_m of the function ψ are determined as

$$\lambda = \frac{1}{2n}\sum_{i=0}^{2n-1}\psi(\frac{i\pi}{n}),\ \ A_m = \frac{1}{n}\sum_{i=0}^{2n-1}\psi(\frac{i\pi}{n})\cos\frac{im\pi}{n}$$

$$B_m = \frac{1}{n}\sum_{i=0}^{2n-1}\psi(\frac{i\pi}{n})\sin\frac{im\pi}{n},\ \ A_n = \frac{1}{n}\sum_{i=0}^{2n-1}(-1)^i\psi(\frac{i\pi}{n})$$

and the function of θ is described with

$$\theta(\varphi) = \varphi + \frac{1}{n}\sum_{k=1}^{2n-1}\psi(\varphi + \frac{k\pi}{n})\,cot\frac{k\pi}{2n},\ \ k = odd$$

$$\theta(\varphi) = \varphi,\quad k = even$$

Note that the function $\theta(\varphi)$ describes the surface angle of airfoils. The conformal mapping from z'-plane to ξ-plane caused by the transformation

$$\xi = \mathrm{z}' + \frac{\epsilon^2}{z\prime}$$

yields a circle in the z-plane into a curve resembling a wing section in the ξ-plane, where $\epsilon = \frac{c}{4}$ (see Fig. 2).

The *c* represents the airfoil chord length. The coordinates of ξ are defined as

$$\xi = \mathrm{x} + \mathrm{iy},$$

which provides the expression of the coordinates of the airfoil with

$$\mathrm{x} = 2\,\epsilon\cosh\psi(\varphi)\cos\theta(\varphi)$$

$$\mathrm{y} = 2\,\epsilon\sinh\psi(\varphi)\sin\theta\,(\varphi)$$

or

$$\mathrm{x} = \left(\mathrm{r} + \frac{\epsilon^2}{r}\right)\cos\theta(\varphi)$$

$$\mathrm{y} = \left(\mathrm{r} - \frac{\epsilon^2}{r}\right)\sin\theta(\varphi).$$

The angle of attack α is defined as the angle between the chord line and incoming wind and can be written by

$$\alpha = tan^{-1}\left(k\frac{y}{x}\right). \qquad (1.1)$$

The k is the value to determine of pitch point and refer to Fig. 2(b).

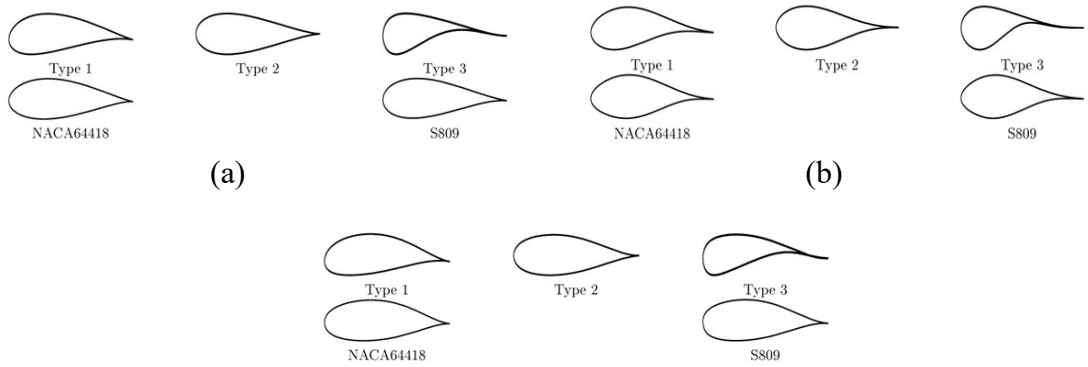

FIGURE 3. Various airfoil profiles: (a) airfoil shapes described by $\theta_1(\varphi)$, (b) airfoil shapes described by $\theta_2(\varphi)$, (c) airfoil shapes described by $\theta_3(\varphi)$.

2.2. **Ideal design and of mean lines**. The mean line is regarded as the locus of midway points between the upper and lower surfaces of the section. Mean lines under the action of a uniformly distributed loading from $x/c = 0$ to $x/c = x^*$ decrease linearly to zero at $x/c = 1$, and the ordinates are expressed as [23]

$$\frac{y}{c} = \frac{C_{l_i}}{2\pi(x^*+1)}\left[k_1\left(\frac{x}{c}\right) + k_2\left(\frac{x}{c}\right)\left(\frac{x}{c} - 1\right) - k_3\left(\frac{x}{c}\right)\frac{x}{c}\right]$$

$$k_1\left(\frac{x}{c}\right) = \frac{1}{1-x^*}\left[\frac{1}{2}\left(x^* - \frac{x}{c}\right)^2 \ln|x^* - \frac{x}{c}| - \frac{1}{2}\left(1 - \frac{x}{c}\right)^2 \ln\left(1 - \frac{x}{c}\right) + \frac{1}{4}\left(1 - \frac{x}{c}\right)^2 - \frac{1}{4}\left(x^* - \frac{x}{c}\right)^2\right] - \frac{x}{c}\ln\frac{x}{c}$$

$$k_2\left(\frac{x}{c}\right) = \frac{1}{1-x^*}\left[x^{*2}\left(\frac{1}{2}\ln x^* - \frac{1}{4}\right) + \frac{1}{4}\right]$$

$$k_3\left(\frac{x}{c}\right) = \frac{1}{1-x^*}\left[\frac{1}{2}(1-x^*)^2 \ln(1-x^*) - \frac{1}{4}(1-x^*)^2\right]. \quad (1.2)$$

The C_{l_i} implies the ideal lift coefficient. The ideal angle of attack α_i for these mean lines is

$$\alpha_i\left(\frac{x}{c}\right) = \frac{C_{l_i}}{2\pi(1+x^*)}\left[k_3\left(\frac{x}{c}\right) - k_2\left(\frac{x}{c}\right)\right]. \quad (1.3)$$

3. RESULTS AND DISCUSSIONS

Three types of $\theta(\varphi)$ and five types of $\psi(\varphi)$ are chosen to describe of angle attack and ideal lift coefficient for various airfoil shapes. The functions chosen are exhibited below, and the airfoil shapes depicted by the chosen functions are displayed in Fig. 3.

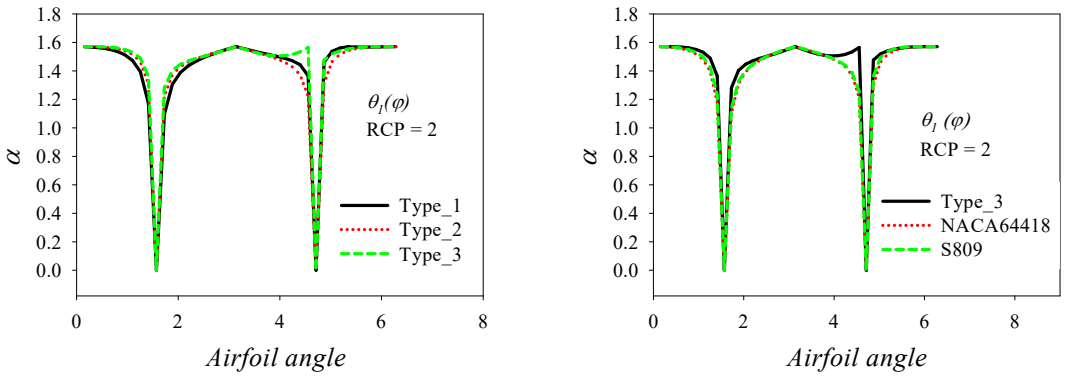

Figure 4. Attack angle for various airfoil profiles described by $\theta_1(\varphi)$.

$$\theta_1(\varphi) = \varphi,$$
$$\theta_2(\varphi) = \varphi - 0.08\sin\varphi + 0.1\cos\varphi - 0.3\sin 2\varphi$$
$$\theta_3(\varphi) = \varphi + 0.05\sin\varphi - 0.05\cos\varphi + 0.05\sin 2\varphi - 0.05\cos 2\varphi - 0.08\sin 3\varphi,$$
$$\psi_1(\varphi) = 0.1(1-\cos\theta_i(\varphi)) + 0.05\sin\theta_i(\varphi)$$
$$\psi_2(\varphi) = 0.05(1-\cos\theta_i(\varphi))^2 + 0.05(\sin\theta_i(\varphi))^2$$
$$\psi_3(\varphi) = 0.03(1-\cos\theta_i(\varphi))^3 + 0.03(\sin\theta_i(\varphi))^3$$
$$\psi_{NACA64418}(\varphi) = 0.89482(1-\cos\theta_i(\varphi)) + 0.04960\sin\theta_i(\varphi) - 0.35665(1-\cos\theta_i(\varphi))^2 - 0.35445(\sin\theta_i(\varphi))^2 - 0.02444(1-\cos\theta_i(\varphi))^3 - 0.01001(\sin\theta_i(\varphi))^3$$
$$\psi_{S809}(\varphi) = 1.47486(1-\cos\theta_i(\varphi)) + 0.04733\sin\theta_i(\varphi) - 0.55641(1-\cos\theta_i(\varphi))^2 - 0.65773(\sin\theta_i(\varphi))^2 - 0.07436(1-\cos\theta_i(\varphi))^3 - 0.05212(\sin\theta_i(\varphi))^3$$

In the figures of results, RCP implies the ratio of x value of conformal transformation to the length of pitch point and W is the relative flow angle onto blade. The absolute value of $\frac{y}{x}$ is used to obtain the positive attack angle in the Eq. (1.1).

Figure 4 shows attack angles for various airfoil profiles, and is divided into two images for a clear comparison. The airfoil shapes are determined by $\theta_1(\varphi)$, and the angles of attack are obtained with the value RCP=2. All type airfoils appear similar aspect in the development of attack angle in overall area, and trivial attack angle occurs at both angles $\varphi = \frac{\pi}{2}$ and $\frac{3\pi}{2}$. The value of attack angle decreases on the both intervals of $(0, \frac{\pi}{2})$ and $(\pi, \frac{3\pi}{2})$, and increases on the both interval $(\frac{\pi}{2}, \pi)$ and $(\frac{3\pi}{2}, 2\pi)$ with the growth of φ. Type 3 airfoil expresses the largest magnitude of attack angle among the other airfoil types, especially over near area of $\frac{3\pi}{2}$. This result implies that the airfoil shape manufactured on the ground of Type 3 reacts most sensitively to the flowing wind.

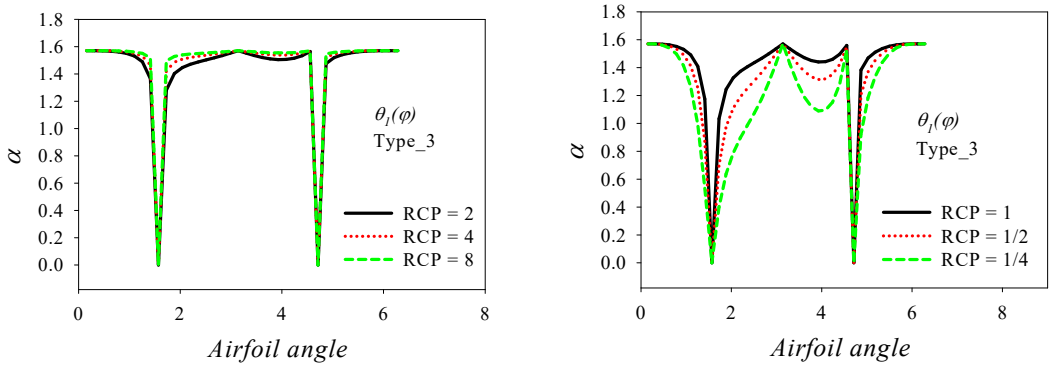

FIGURE 5. Attack angle of Type 3 airfoil described by $\theta_1(\varphi)$ for various pitch points: (a) RCP >1, (b) 0 < RCP < 1.

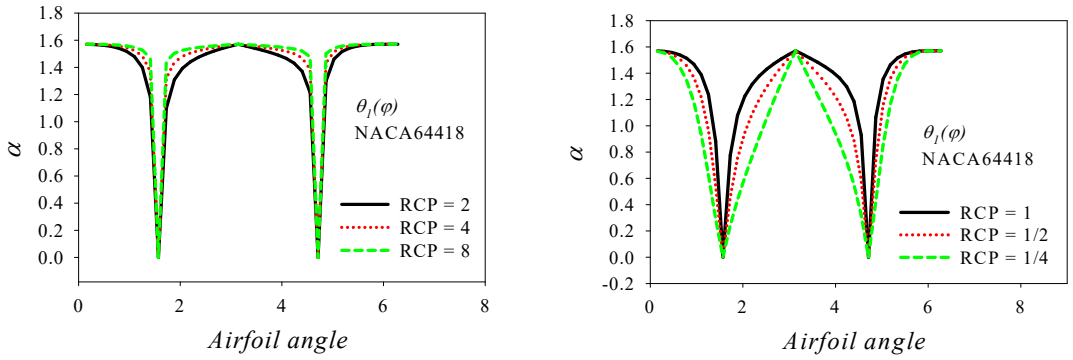

FIGURE 6. Attack angle of NACA64418 airfoil described by $\theta_1(\varphi)$ for various pitch points: (a) RCP >1, (b) 0 < RCP < 1.

Through Figs. 5~7, attack angles of Type 3, NACA64418, and S809 airfoil profiles are depicted for various pitch points. The selected values of RCP are $\frac{1}{4}, \frac{1}{2}, 1, 2, 4, 8$. Figure 5 portrays the attack angle distributions of Type 3 airfoil profiles described by $\theta_1(\varphi)$. As shown in Figs. 5(a) and 5(b), the attack angle distributions surge with further fluctuation as RCP value decreases, which signifies that airfoil shape with smaller RCP value is more susceptible to the upcoming wind. But, the magnitude of attack angle is getting smaller with the decay of RCP, and the variation of angle attack meager in Type 3 airfoil of RCP ≥ 4. Figs. 6 and 7 represent the angles of attack for NACA64418 and S809 airfoil profiles, respectively. The magnitude of attack angle distribution is getting larger as the value of RCP grows on both NACA64418 and S809 airfoil shapes. But, unlike Type 3 airfoil, there is no variation in the number of distribution fluctuation. On the whole the decline of RCP value induces smaller angle of attack in magnitude, which implies that airfoil profile possessing pitch point close to the airfoil tip reacts weakly to upcoming wind.

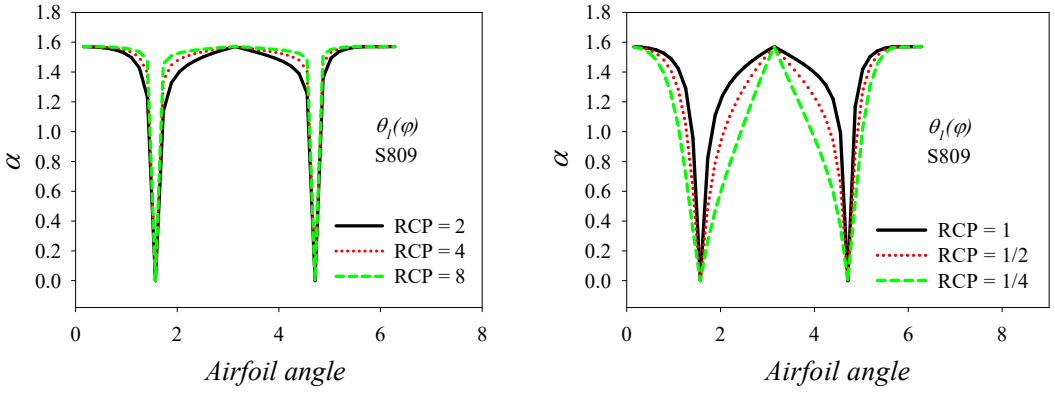

FIGURE 7. Attack angle of S809 airfoil described by $\theta_1(\varphi)$ for various pitch points: (a) RCP >1, (b) 0 < RCP < 1.

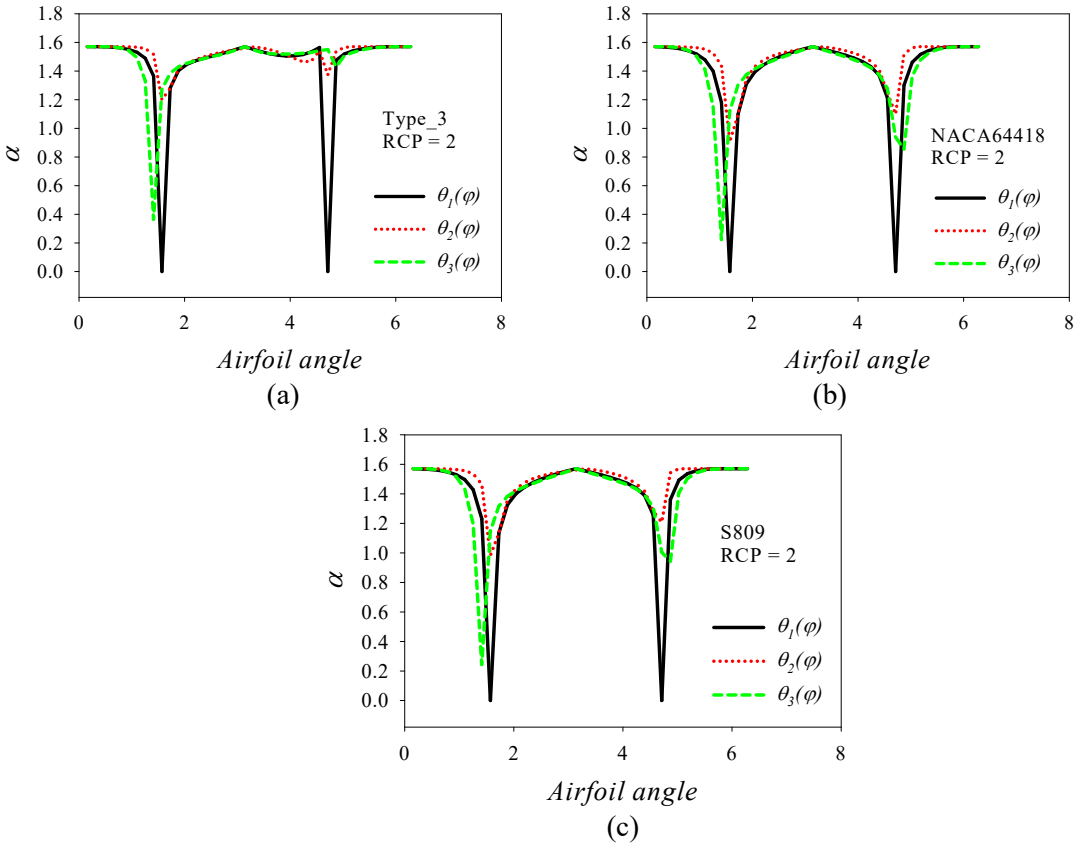

FIGURE 8. Attack angle of airfoil profiles at RCP=2 for various functions $\theta(\varphi)$: (a) Type 3 airfoil, (b) NACA64418 airfoil, (c) S809 airfoil.

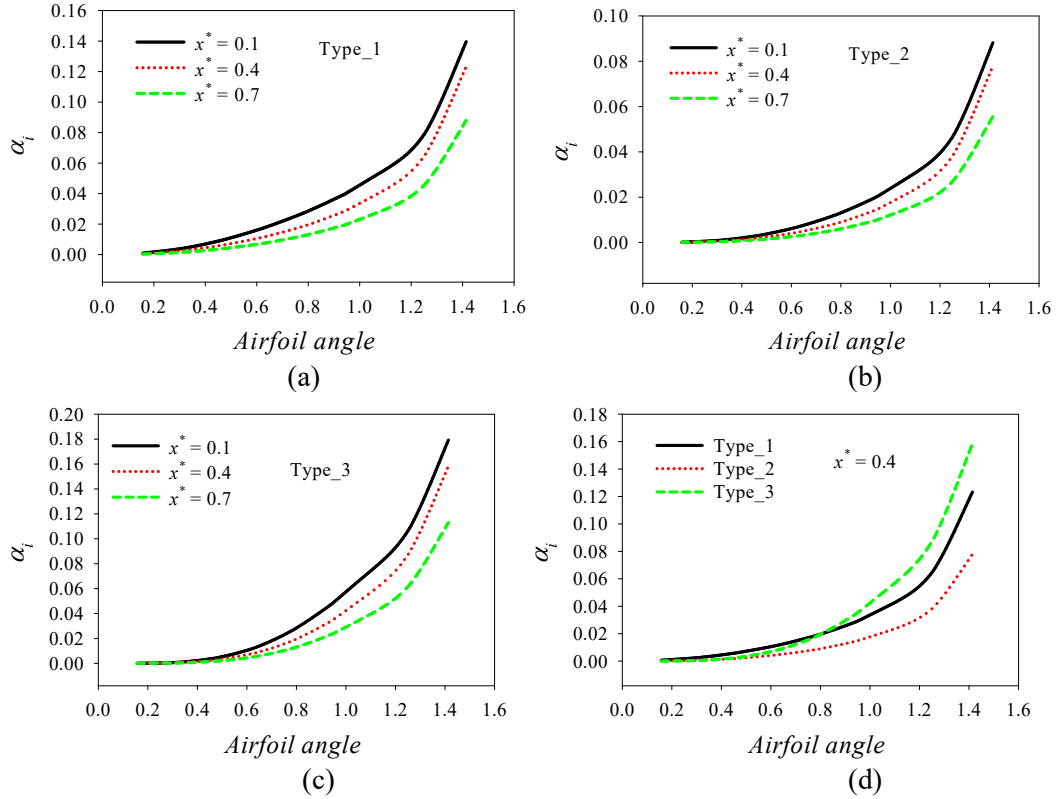

FIGURE 9. Ideal attack angle: (a) for various airfoil profiles at $x^* = 0.4$, (b) Type 1 airfoil, (c) Type 1 airfoil, (d) Type 1 airfoil.

Figure 8 displays the distributions of attack angle for various surface function $\theta(\varphi)$ with RCP=2. As shown in Figure, the surface function $\theta_3(\varphi)$ yields the smallest attack angle distribution over the interval $(0, \frac{\pi}{2})$ for the airfoil profiles of Type 3, NACA64418, and S809 airfoil. The largest magnitude of attack angle distributions appears in the airfoil profiles manufactured with function the function $\theta_3(\varphi)$ in almost every domain, while the function $\theta_1(\varphi)$ provides the smallest attack angle over the interval $(\frac{\pi}{2}, 2\pi)$. NACA64418 airfoil profiles are affected the least in the choice of function $\theta(\varphi)$ among them over the entire domain. It is recognized through the Fig. 8 that the function $\theta(\varphi)$ representing the conformed surface angle is crucial factor in the determination of angle of attack. In other words, the surface angle of airfoil shape plays an important role to decide the angle of attack.

Ideal attack angle distributions of airfoil profiles of Type 1, Type 2, and Type 3 are obtained using Eq. (1.3), and the results are exhibited in Fig. 9. Representative uniform loading limit values x^* are 0.1, 0.3, and 0.7. Fig. 9(a) explains the ideal angle of attack of Type 1 airfoil shape. The ideal attack angle is decreases as the area suffering uniform loading increases, and the maximum ideal attack angle is around 0.15 of x^*=0.1. Similar tendency appears in Type 2 and Type 3 airfoil profiles, while the maximum ideal attack angles are 0.09 and 0.18, respectively (see Figs. 9(b) and 9(c)). A comparison of ideal attack angle is displayed in Fig.

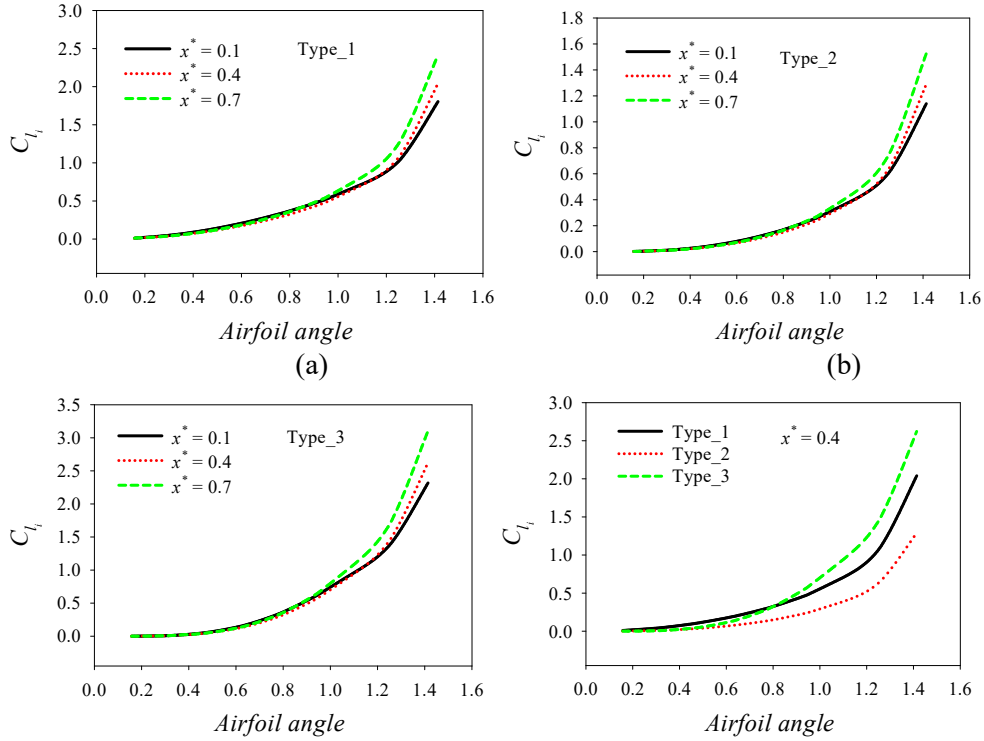

FIGURE 10. Ideal lift coefficient: (a) for various airfoil profiles at $x^* = 0.4$, (b) Type 1 airfoil, (c) Type 1 airfoil, (d) Type 1 airfoil.

9(d) at x^*=0.4. Type 1 airfoil shape expresses the greatest ideal attack angle over interval (1, 0.8), whereas the largest ideal attack angle occurs with Type 3 airfoil shape over interval (0.8, 1.6). The results signify that the Type 1 airfoil shape reacts most pliably to upcoming wind over interval (0, 0.8), and Type 3 airfoil profile over interval (0.8, 1.6).

Equation (1.2) determines ideal lift coefficient distributions of airfoil profiles of Type 1, Type 2, and Type 3, and the obtained results are depicted in Fig. 10. Representative uniform loading limit values $x^* = 0.1, 0.3,$ and 0.7 are chosen. As shown in Fig. 10(a), marginal difference appears over the interval (0.1, 1.0), and ideal lift coefficient grows with the increment of the value x^* over interval (1.0, 1.6). The airfoil under the action of uniform loading to $x^* = 0.7$ creates the largest ideal lift coefficient of around 2.5. Airfoil shapes of Type 2 and Type 3 profiles display similar aspect to Type 1 airfoil in ideal lift coefficient distributions (see Figs. 10(b) and 10(c)). Ideal lift coefficient distributions are compared in Fig. 10(d) with the limit value x^*= 0.4. The airfoil of Type 1 shape represents the highest ideal lift coefficient over interval (0.1, 0.8), whereas the largest ideal lift coefficient is acquired in Type 3 airfoil shape over interval (0.8, 1.6). According to the obtained results, on the whole, Type 3 airfoil shape involves high possibility to generate larger electric energy due to the greater ideal lift coefficient distribution.

4. Conclusions

In this study analytical analysis has been developed to investigate attack angle and ideal lift coefficient distributions for various airfoil profiles in wind turbine blade. Pitch point and uniform loading area are taken into account, and airfoil shape functions of wind turbines and surface angle functions of airfoil are expressed with series using conformal transformations. A method of conformal transformation functions using a trigonometric series form has been proposed the followings:

- Angle distributions of attack appear with various forms depending on the conditions of airfoil shape, pitch point, and surface angle function.
- Airfoil shape reacts sensitively to the flowing wind.
- Airfoil profile possessing pitch point close to the airfoil tip reacts weakly to upcoming wind.
- Conformed surface angle is crucial factor in the determination of angle of attack.
- Ideal attack angle and ideal life coefficient are very sensitive to the variation of uniform loading area.

Through results obtained the determination of proper pitch point, loading area, and airfoil shape are essential factors to control the angle of attack, and the results may be useful in designing wind turbine airfoils.

Acknowledgments

This research was supported by Dong-A University.

Data Availability Statement

The data used to support the findings of this study are available from the corresponding author upon request.

Conflicts of Interest

The author declares that there are no conflicts of interest.

References

[1] GWEC, Global Wind Report, 2016.
[2] J.F. Manwell, J.G. McGowan, A.L. Rogers, *Wind Energy Explained: Theory, Design, and Application*, John Wiley & Sons, West Sussex, 2010.
[3] X. Tang, *Aerodynamic Design and Analysis of Small Horizontal axis Wind Turbine Blades*, University of Central Lancashire, UK, 2012.
[4] E. Branlard, *Wind Turbine Tip-loss Corrections: Review, Implementation and Investigation of New Models*, RisoDTU (Technical University of Denmark), Lyngby, Denmark, 2011.
[5] J.G. Leishman, *Challenges in modelling the unsteady aerodynamics of wind turbines*, Wind Energy, **5(2-3)** (2002), 85-132.
[6] S. Gupa, *Development of a Time-accurate Viscous Lagrangian Vortex Wake Model for Wind Turbine Applications*, University of Maryland, 2006.
[7] O. Turhan and G. Bulut, *On nonlinear vibrations of a rotating beam*, Journal of Sound and Bibration, **322(1-2)** (2009), 314-335.

[8] R.M. Hicks, E.M. Murman, G.N. *Vanderplaats, An assessment of airfoil design by numerical optimization*, NASA TM X-3092, 1974.
[9] R. Eppler and D.M. Somers, *A computer program for the design and analysis of low-speed airfoils*, NASA TM-80210, 1980.
[10] J.L. Tangler, D.M. Somers, *NREL airfoil families for HAWT's*, NREL, United States 1995.
[11] S. Sarkar and H. Bijl, *Nonlinear aeroelastic behavior of an oscillating airfoil during stall-induced vibration*, Journal of Fluids and Structures, **199(6)** (2008), 757-777.
[12] D.N. Srinath and S. Mittal, *Optimal aerodynamic design of airfoils in unsteady viscous flows*, Computer Method in Applied Mechanics and Engineering, **99(29-32)** (2010), 1976-1991.
[13] I. Echjijem and A. Djebli, *Design and optimization of Wind Turbine with Axial Induction Factor and Tip Loss Corrections*, Procedia Manufacturing, **46** (2020), 708-714.
[14] H. Lim and H. Kim, *Multi-objective airfoil shape optimization using an adaptive hybrid evolutionary algorithm, Aerospace Science and Technology*, **87** (2019), 141-153.
[15] M.R. Tirandaz and A. Rezaeiha, *Effect of airfoil shape on power performance of vertical axis wind turbines in dynamic stall: Symmetric Airfoils*, Renewable Energy, **173** (2021), 422-441.
[16] H. Hu, G. Zhang, D. Li, Z. Zhang, T. Sun, and Z. Zong, *Shape optimization of airfoil in ground effect based on free-form deformation utilizing sensitivity analysis and surrogate model of artificial neural network*, Ocean Engineering, **257** (2022), 111514.
[17] L. Sartori, F. Grasso, C. Bottasso, A. Croce, *Integration of airfoil design during the design of new blades*, Technical University of Denmark, Proceedings of ICOWES 2013, Lyngby, Danmark 2013.
[18] X. Wang, L. Wang, and H. Xia, *An Integrated Method for Designing Airfoils Shapes, Mathematical problem in Engineering*, **2015**, 838674.
[19] J.Z. Wei, Z.S. Wen, S.N. Jens, *Integrated airfoil and blade design method for large wind turbines*, Renewable Energy, **70** (2014), 172-183.
[20] K. Kumar, O.P. Mishra, and S. Kumar, *Simulation of Airfoil Shape for Optimum Wing Characteristics*, Material Today: Proceedings **24** (2020), 2231-2237.
[21] S. Huang, H. Qiu, Y. Wang, *Aerodynamic performance of horizontal axis wind turbine with application of dolphin head-shape and lever movement of skeleton bionic airfoils*, Energy Conversion and Management, **267** (2022), 115803.
[22] M. N$\acute{u}\tilde{n}$ez, *On the shape of the cavity created by a thin magnetized airfoil*, Physics Letters A, **448** (2022), 128322.
[23] I.H. Abbott and A.E.V. Doenhoff, *Theory of Wing Sections, Dover Publications*, New York, 1958.